Estimation of Grinding Force with Consideration of Rupture Factor

IOP Conf. Series: Materials Science and Engineering 470 (2019) 012027 doi:10.1088/1757-899X/470/1/012027

Estimation of Grinding Force with Consideration of Rupture Factor

Jianliang Guo*, Jun Chi and Lianqing Chen

School of Mechanical Engineering, Ningbo University of Technology, Ningbo, 315336, China

*guojianliang76@gmail.com, +86-13857879737

Abstract. Grinding force has been treated as an indication of the accuracy and surface quality of ground workpiece. Building a model which can be used to estimate or predict accurately the grinding force will allow us to monitor indirectly and on-line the accuracy and surface quality of grinding, which lays the foundation for implementation of intelligent grinding. Based on analysis of stress concentration in this work, a model of grinding force is proposed, in which the rupture factor of chip at the interface between the grain and workpiece is considered quantitatively and independently. The effect of stress concentration on the grinding force is included in the rupture factor. Least square method and experimental tests under orthogonal test design are used to determine the coefficients in the model. The model is validated through additional experimental tests and the results show that the average prediction accuracy reaches 81.42% for specific normal grinding force and 78.58% for specific tangential grinding force, and the trend in the measured results was well predicted by the proposed model.

1. Introduction

Because of the multiplicity of cutting points and their irregular geometry, the high cutting speeds, and the small depths of cut which vary from grain to grain, any attempt to analyze the mechanisms of grinding might appear to be a hopeless task [1]. Based on some simplification or assumption, a model can be constructed and then used as an entry to describe the complicated physical laws in grinding process. In fact, in international research the modeling and simulation of processes is established as an excellent tool for assessing and optimizing grinding processes [2]. Industrial practice shows that grinding force is closely related to the final accuracy and surface quality of the products. Generally, high normal component of grinding force causes erratic part tolerance and self-induced vibration of the grinding system while high tangential component leads to high grinding heat generation and consequently thermal damage of the workpiece. Building a realistic model and hence estimating the force before the actual grinding process would allow the grinding performance to be evaluated and optimized in advance, which would also be quite helpful to the implementation of intelligent grinding in the future.

A number of models have been developed in the literature to describe analytically or empirically the grinding force, in which the stochastic nature of grinding process was generally taken into account. Badger and Torrance developed a 2-D model and a 3-D model to predict grinding force respectively [3], both of which consider the grit-workpiece interface as a rigid plastic contact whose behavior depends on the asperity slope distribution and the interfacial coefficient of friction obtained from wheel profiles. Karkalos et al. employed regression analysis and artificial neural networks to model

and predict grinding forces respectively [4]. Chang and Wang formulated the dynamic grinding force as the convolution of a single-grit force and the grit density function [5]. In the frequency domain, the power spectrum density of the grinding force was deduced to be the product of the energy spectrum density of the single-grit force and the power spectrum density of the grit density function. The single-grit force was modeled to be a deterministic impulse response of the grinding process. Mishra and Salonitis compared several existing models in the relevant literature [6], and then made some slight modifications to one of them to obtain the best description of grinding force in advanced grinding processes such as creep-feed grinding and high-efficiency deep grinding. Based on an undeformed chip thickness model, Agarwal and Rao built a stochastic model of grinding force which considers the real contact length in terms of the elastic properties of the wheel and workpiece material and other grinding parameters [7]. Karkalosa et al. conducted a molecular dynamics simulation of nanometric peripheral grinding to determine the grinding force [8]. They found that grinding forces increased about two times at larger depth of cut whereas a much smaller variation was reported for grinding speed variation. Zhang et al. presented a theoretical force model by considering the material-removal mechanism, the plastic-stacking mechanism, and also the influence of lubricating conditions [9], in which the aggregate force was derived through the synthesis of each single-grain force. Durgumahanti et al. presented a model of grinding force by incorporating the effects of variable coefficient of friction and the plowing force [10], based on the fact that the coefficient of friction varies with the process parameters and the plowing force would become more predominant at very low depth of cuts.

Due to the stochastic nature of grinding process, which gives rise to a lot of complicated influencing factors on grinding force, several coefficients are usually employed in the existing models to represent the effects of the undiscovered influencing factors. It would be helpful to make clear all these undiscovered factors in grinding force model step by step for predicting grinding force. If the quantitative contribution of the unknown factors can be identified, then the research of grinding mechanism will be pushed forward considerably. Also, understanding these factors will allow us to make ideal design for the grinder and to optimize the grinding process parameters, which avoids the material and energy waste resulted from the commonly used conservative design nowadays. As one of the unknown factors, stress concentration was seldom discussed in the literature due to its complicated development mechanism. Generally, stress concentration dictates partly how easily the material can be cut off by the grains during grinding operation. Consequently it would improve the comprehensiveness of the existing grinding force models to characterize the contribution of stress concentration to grinding force. Only Lin et al. was found to establish a model of grinding force based on stress concentration theory [11]. However, Lin et al. did not consider the stress concentration phenomenon within the plastic region [11], which actually occurs during the chip formation. Also, Lin et al. did not relate systematically the grain geometry to the shape and size of the notch at the interface between the grain and workpiece [11], which is the foundation of the effect of stress concentration on the grinding force. Considering this, through the analysis of the rupture factor in which the effect of stress concentration within the plastic region is included, we improved the grinding force model proposed by Durgumahanti et al. [10].

2. Grinding force model

Durgumahanti et al. proposed a grinding force model shown in Eq. (1) and (2) [10], in which both the specific normal force Fn' and specific tangential force Ft' are separated into the chip formation force, friction force, and plowing force.

$$F_n^{'} = K_1 \frac{v_w}{v_s} a_p + K_2 \frac{v_w}{v_s} \left(\frac{a_p}{d_e} \right)^{1/2} + K_3 \left(\frac{v_w}{v_s} \right)^{a_0} (d)^{b_0} (a_p)^{c_0} C_s (a_p d_e)^{1/2} \tag{1}$$

$$F_t^{'} = K_4 \frac{v_w}{v_s} a_p + \left(K_5 + K_6 \frac{v_w}{d_e v_s} \right) (a_p d_e)^{1/2} + K_7 \left(\frac{v_w}{v_s} \right)^{a_0} (d)^{b_0} (a_p)^{c_0} C_s (a_p d_e)^{1/2} \tag{2}$$

The chip formation process can essentially be described using the model of metal cutting as shown in Fig. 1. Within the shear slip plane OM, the material stress progressively increases until the chip forms and breaks from the workpiece. Fig. 2 presents the development of the correlation of stress and strain.

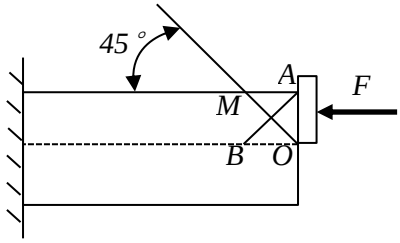

Figure 1. Model of metal cutting

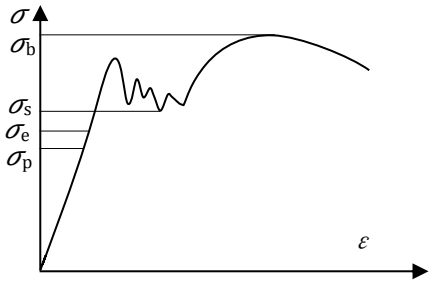

Figure 2. Deformation curve of metal cutting

During the chip formation process, phenomenon of stress concentration occurs in the contact zone of an active grain and the workpiece. Basically the interaction between an individual grain and the workpiece is considered to be quite similar to geometrically defined cutting process like turning or milling process except that the grain has a negative rake angle. As shown in the equivalent approximation of the interaction in Fig. 3, the abrasive grit acts as an indenter and squeezes gradually the material to form a shallow notch, which leads to stress concentration with the largest stress occurring at the bottom of the notch. Based on this feature of stress concentration, the small portion of material surrounding the notch can be equivalently characterized by the tensile model of a plate with a shallow notch shown in Fig. 4. In this model, the ρ denotes the curvature radius at the bottom of the notch. The t represents the depth of the notch. The σ_0 is the reference stress, which occurs far away from the notch.

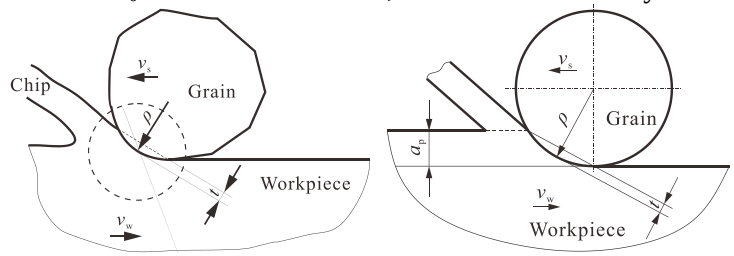

(a) Actual interaction (b) Equivalent approximation of the interaction

Figure 3. Approximation of the interaction of abrasive grain and workpiece.

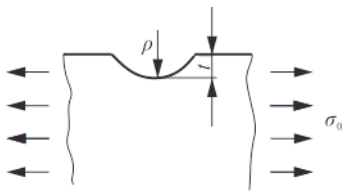

Figure 4. Tensile model of the Interaction

The radius ρ of curvature at the notch bottom can be approximated to be the equivalent radius of the grain. The depth t of notch can be determined through geometrical relationship in Fig. 1.

Li et al. presents the stress concentration factor α corresponding to the model in Fig. 4 [12].

$$\alpha = \frac{\sigma_{\max}}{\sigma_0} = 1 + 2\sqrt{\frac{t}{\rho}} \tag{3}$$

in which the $\sigma_{\max}$ represents the maximum stress which occurs at the bottom of the notch. The t can be determined from Fig. 1.

$$t = \rho - \sqrt{\rho^2 - \frac{\rho a_p}{2}} \tag{4}$$

Due to the fact that the notch generates from the squeezing action of the abrasive grit, it is reasonable to consider ρ to be equal to the radius of the abrasive grit. In fact, each nominal grit number M corresponds to a range of grit size, but the grit dimension for a specific grinding wheel might be characterized by the average value d of the grit sizes. Malkin and Guo give the average value in Eq. (5) [1], in which the d is defined to be 60% of the average spacing between adjacent wires in a sieve whose mesh number equals the grit number M.

$$d = 15.2M^{-1} \tag{5}$$

Consequently, the curvature radius ρ can be assigned as

$$\rho = 7.6M^{-1} \tag{6}$$

It should be noted that the expression of stress concentration factor in Eq. (3) is based on the assumption that the deformation of workpiece material does not go beyond the elastic region throughout the grinding process. However, during actual grinding process the chip formation would go through successively the elastic deformation region, the elastic-plastic deformation region, the plastic deformation region, and finally lead to the rupture. This means that only when the maximum stress σ_{max} at the bottom of the notch does not exceed the yield strength σ_s, the stress concentration factor can be determined using Eq. (3). But when the σ_{max} exceeds the yield strength, the stress field will be redistributed so that the ratio of σ_{max} to σ_0 will be different from the ratio in elastic region. Apart from this, the phenomenon of work hardening also has an impact on the σ_{max} to some extent. Like other metal-cutting processes, material removal by grinding involves a shearing process of chip formation [1]. When the shear slip generates within the workpiece material, the work hardening increases the shear slip resistance and hence the failure strength will also be increased. This means that the description of the actual stress state that leads to chip formation entails considering comprehensively all the above-mentioned influencing factors. The rupture factor β acts as a parameter involving these influencing factors, and hence is taken into account to determine the specific chip formation force in this work. As such, the expressions of the specific normal chip formation force F_{nc}' and the specific tangential chip formation force F_{tc}' in Eq. (1) and (2) would be improved to become Eq. (7) and (8) respectively.

$$F_{nc}^{'} = \frac{1}{\beta}\left(\frac{K_1^{'} v_w}{v_s} a_p\right) \tag{7}$$

$$F_{tc}^{'} = \frac{1}{\beta}\left(\frac{K_4^{'} v_w}{v_s} a_p\right) \tag{8}$$

in which the K_1' and K_4' are the undetermined coefficients. Neuber formula relates β to the stress concentration factor α as shown in Eq. (9) [12].

$$\beta = 1 + \frac{\alpha - 1}{1 + \sqrt{\frac{\varepsilon_0}{\rho}}} \tag{9}$$

in which ε_0 is a constant which is equal to 0.48 mm for mild steel.

Another mechanism associated with grinding process is plowing. Plowing usually refers to the side flow of material from the cutting path into ridges shown in Fig. 5. From Fig. 5, it can be observed that material breakage and stress concentration also occur in the plowing process. Thus the normal and tangential plowing force components in Eq. (1) and (2) can be revised to be Eq. (10) and (11).

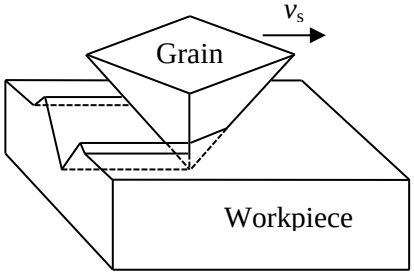

Figure 5. Illustration of plowing

$$F_{np}^{'} = \frac{1}{\beta} K_3^{'} \left(\frac{v_w}{v_s}\right)^{a_0} (d)^{b_0} (a_p)^{c_0} C_s (a_p d_e)^{1/2} \tag{10}$$

$$F_{tp}^{'} = \frac{1}{\beta} K_7^{'} \left(\frac{v_w}{v_s} \right)^{a_0} (d)^{b_0} (a_p)^{c_0} C_s (a_p d_e)^{1/2} \tag{11}$$

So far, the equations in [10] for the specific normal and tangential grinding force can be rewritten to be

$$F_n^{'} = \frac{\sqrt{\rho}+\sqrt{\varepsilon_0}}{\alpha\sqrt{\rho}+\sqrt{\varepsilon_0}} \left(\frac{K_1^{'} v_w}{v_s} a_p \right) + \frac{K_2^{'} v_w}{v_s} \left(\frac{a_p}{d_e} \right)^{1/2} + K_3^{'} \frac{\sqrt{\rho}+\sqrt{\varepsilon_0}}{\alpha\sqrt{\rho}+\sqrt{\varepsilon_0}} \left(\frac{v_w}{v_s} \right)^{a_0} (d)^{b_0} (a_p)^{c_0} C_s (a_p d_e)^{1/2} \tag{12}$$

$$F_t^{'} = \frac{\sqrt{\rho}+\sqrt{\varepsilon_0}}{\alpha\sqrt{\rho}+\sqrt{\varepsilon_0}} \left(\frac{K_4^{'} v_w}{v_s} a_p \right) + \left(K_5^{'} + \frac{K_6^{'} v_w}{d_e v_s} \right) (a_p d_e)^{1/2} + K_7^{'} \frac{\sqrt{\rho}+\sqrt{\varepsilon_0}}{\alpha\sqrt{\rho}+\sqrt{\varepsilon_0}} \left(\frac{v_w}{v_s} \right)^{a_0} (d)^{b_0} (a_p)^{c_0} C_s (a_p d_e)^{1/2} \tag{13}$$

in which the values of plowing force coefficients a_0, b_0, c_0, and C_s are taken identical to those in [10], which were determined through the single-grit test and the imprint test. This is because that these coefficients are dependent on the workpiece material and the grinding wheel composition and the same workpiece material and the grinding wheel composition are used in this work as in [10]. The remaining coefficients K_1', K_2', K_3', K_4', K_5', K_6' and K_7' will be determined through grinding experiments.

3. Coefficient determination and model validation

3.1. Experimental scheme and setup

For determining the model coefficients and then validating the model, a total number of 26 experimental tests in surface grinding configuration were performed. Firstly, the coefficients were determined by using 16 experimental tests given in Table 1, which consists of three variables and four levels arranged under orthogonal test design. Afterwards, the prediction accuracy of the model was estimated through another 10 experimental tests with randomly selected values of the parameters shown in Table 3.

Table 1. Experiments for identifying model coefficients.

Exp. no.	a_p (mm)	v_w (m/min)	v_s (m/s)	$F_n^{'}$ (N/mm)	$F_t^{'}$ (N/mm)
1	0.01	5	21	7.53	3.59
2	0.01	10	24	11.61	5.61
3	0.01	15	27	18.15	5.58
4	0.01	20	30	22.88	5.61
5	0.02	5	24	11.26	6.27
6	0.02	10	21	25.19	9.92
7	0.02	15	30	22.32	9.26
8	0.02	20	27	34.60	12.25
9	0.03	5	27	14.65	8.88
10	0.03	10	30	21.19	10.94
11	0.03	15	21	46.84	14.13
12	0.03	20	24	45.67	17.45
13	0.04	5	30	18.02	9.39
14	0.04	10	27	30.87	12.54
15	0.04	15	24	52.04	16.88
16	0.04	20	21	71.38	25.71

The grinding experiments have been conducted on a self-developed surface grinding machine using the aluminum oxide grinding wheel A60M6V with an outer diameter of 350 mm and a width of 40 mm. Before each grinding experiment, the dressing operation was carried out by using a single point diamond tool with a dressing depth of 0.02 mm. The axial feed rate of the dressing tool per wheel revolution was 0.04 mm/r. Two spark-out passes were taken after each dressing operation. The workpieces were made of mild steel 20# (Chinese model) with a dimension of 40×20×20 mm^3. Normal and tangential grinding forces were measured throughout each test. The data were not recorded until the forces reached a steady-state value. Usually the dynamometer for grinding operation can be divided into the strain type and the

piezoelectric type. The strain dynamometer is especially good for measuring the static force or the slowly varying force, whereas the piezoelectric dynamometer cannot be used for measuring the static force because it is of alternating current coupling. In this work the strain dynamometer was adopted to measure the grinding force under the scheme shown in Fig. 6. The workpiece is held on the strain dynamometer, in which a strain foil is bonded to an elastic body. As the grinding force acts on the elastic body, a deformation occurs on the elastic body and an identical elastic deformation is transferred to the strain foil. The deformation leads to a change in resistance value of the strain foil. The resistance strain gauge is used to transform this change in resistance value into a small electric signal and then to amplify it. Finally, the amplified electric signal is obtained by the industrial personal computer using the data acquisition card for the following storage and processing.

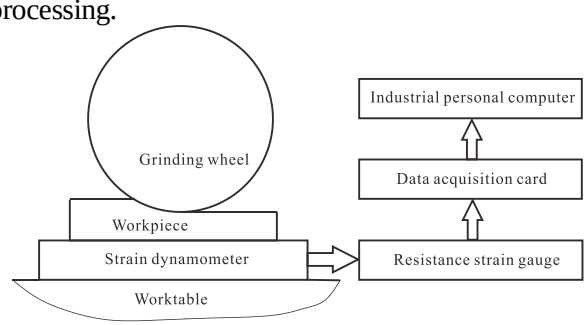

Figure 6. Scheme of measuring the grinding force

3.2. Identification of the model coefficients

As shown in Table 1, the 16 experiments are intended to obtain the values of the model coefficients K_1', K_2', K_3', K_4', K_5', K_6' and K_7'. The considered process variables are the depth of cut a_p, the workpiece velocity v_w, and the grinding wheel velocity v_s. Eq. (14) and (13) use the least square method to identify the coefficients K_1', K_2', K_3', K_4', K_5', K_6' and K_7' in Eq. (12) and (13).

$$\begin{cases} \dfrac{\partial}{\partial K_1'}\sum_{i=1}^{16}\left(F_{n,ip}' - F_{n,im}'\right)^2 = 0 \\ \dfrac{\partial}{\partial K_2'}\sum_{i=1}^{16}\left(F_{n,ip}' - F_{n,im}'\right)^2 = 0 \\ \dfrac{\partial}{\partial K_3'}\sum_{i=1}^{16}\left(F_{n,ip}' - F_{n,im}'\right)^2 = 0 \end{cases} \tag{14}$$

in which $F_{n,ip}'$ and $F_{n,im}'$ refer to the ith predicted and the ith measured specific normal grinding force respectively.

$$\begin{cases} \dfrac{\partial}{\partial K_4'}\sum_{i=1}^{16}\left(F_{t,ip}' - F_{t,im}'\right)^2 = 0 \\ \dfrac{\partial}{\partial K_5'}\sum_{i=1}^{16}\left(F_{t,ip}' - F_{t,im}'\right)^2 = 0 \\ \dfrac{\partial}{\partial K_6'}\sum_{i=1}^{16}\left(F_{t,ip}' - F_{t,im}'\right)^2 = 0 \\ \dfrac{\partial}{\partial K_7'}\sum_{i=1}^{16}\left(F_{t,ip}' - F_{t,im}'\right)^2 = 0 \end{cases} \tag{15}$$

in which $F_{t,ip}'$ and $F_{t,im}'$ refer to the ith predicted and the ith measured specific tangential grinding force respectively. Solving Eq. (14) and (15) gives the values of the model coefficients shown in Table 2.

Table 2. Values of model coefficients.

K_1'	K_2'	K_3'	K_4'	K_5'	K_6'	K_7'
97961	166950	14.30	39564	5780	0.08	15.73

3.3 Model validation and result discussion

Table 3 gives the parameter values of the ten experimental tests for validating the model. The predicted grinding force was compared with the corresponding measured result in Fig. 7. It can be observed that the correlation between the predicted and measured grinding forces is adequate with an average prediction accuracy of 81.42% for the specific normal grinding force and 78.58% for the specific tangential grinding force, and that the trend in the measured results was well predicted by the proposed model.

Table 3. Experiments for model performance test.

Exp. no.	a_p (mm)	v_w (m/min)	v_s (m/s)
1	0.03	15	27
2	0.04	6	21
3	0.01	18	23
4	0.04	19	31
5	0.03	15	22
6	0.01	16	28
7	0.02	16	27
8	0.03	11	24
9	0.04	15	30
10	0.04	8	21

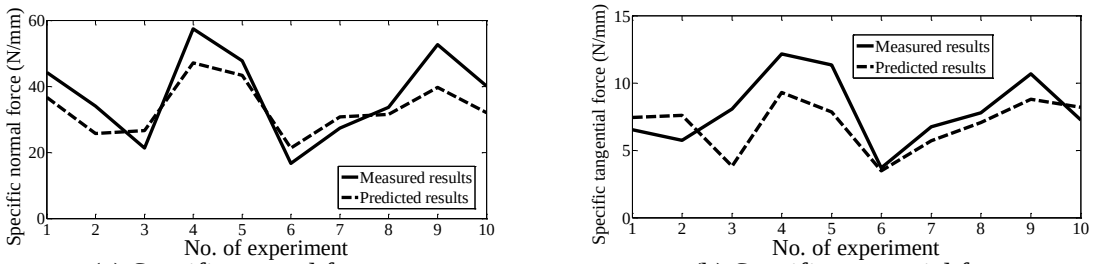

(a) Specific normal force (b) Specific tangential force

Figure 7. Comparison between the measured and predicted grinding force.

There are several possible explanations for the deviation between the predicted and measured values. One reason probably results from the limitation of the available theory in the area of stress concentration. The model shown in Fig. 4 was employed because it can be used as an entry point to explore the regime of the stress concentration in grinding. However, it should be noted that it can not perfectly explain some of the actual phenomena within the grinding zone. For example, as shown in Fig. 4, the stress concentration within the interface of the grain and the workpiece was assumed to be a two-dimension problem. This means that the stress and strain distribution along the third dimension is uniform. In reality, due to the irregular geometry of the grains along with the tiny size of them, the distribution is not probably uniform along the third dimension. Therefore, the effectiveness of the above assumption would be deteriorated by the boundary effects to some extent.

Secondly, throughout the grinding process, self-sharpening of the wheel continues with the generation of wear flats and stochastic grit pullout, which means that the interface conditions between the wheel and workpiece is continuously changing. The effective contact area between the grain and workpiece and the attack angle of the grain are changing all the time accordingly. The magnitude of the grinding force would be inevitably affected by the changes in the contact area and the attack angle. Unfortunately, these influencing factors are not yet able to be considered independently in the proposed model due to the limited conditions.

Another reason of the prediction deviation is due to the temperature rise in grinding zone, which leads to a variation in hardness of the workpiece surface and a variation in friction coefficient between the workpiece and the wheel. The variation of workpiece hardness and friction coefficient will generate a change in grinding force.

4. Conclusion

Based on the model from [10], an improved model for estimating the grinding force is proposed with quantitative and independent consideration of the rupture factor at the interface between the grain and workpiece, in which the contribution of stress concentration is included. The experimental results show that the average prediction accuracy of the model reaches 81.42% for the specific normal grinding force and 78.58% for the specific tangential grinding force, and the trend in the measured results was well predicted by the proposed model. For further improving the prediction accuracy, the remaining important influencing factors need to be considered independently, which include the boundary condition of the stress concentration model, the effects of self-sharpening, and the temperature rise in the grinding zone.

Acknowledgments
This work was supported by the Ningbo Natural Science Foundation of P. R. China under Grant number 2015A610149 and the Zhejiang Provincial Natural Science Foundation of P. R. China under Grant number LY14E050003.

Nomenclature
F_n': Specific normal grinding force
F_t': Specific tangential grinding force
K_1, K_2, K_3, K_4, K_5, K_6, K_7, a_0, b_0, c_0, K_1', K_2', K_3', K_4', K_5', K_6' K_7': Undetermined coefficient
a_p: Depth of cut
v_w: Workpiece feed speed
v_s: Wheel speed
d: Diameter of the grit
d_e: Equivalent wheel diameter
C_s: Number of grains per unit area
α: Stress concentration factor
σ_{max}: Maximum stress
σ_0: Reference stress
σ_p: Proportional limit
σ_e: Elastic limit
σ_s: Yield limit
σ_b: Ultimate strengh
t: Depth of the notch
ρ: Curvature radius of the notch
M: Grit number
σ_s: Yield strength
β: Rupture factor
F_{nc}': Specific normal chip formation force
F_{tc}': Specific tangential chip formation force
ε_0: A constant
$F_{n,ip}'$: The ith predicted specific normal grinding force
$F_{n,im}'$: The ith measured specific normal grinding force
$F_{t,ip}'$: The ith predicted specific tangential grinding force
$F_{t,im}'$: The ith measured specific tangential grinding force

References
[1] Malkin, S. and Guo, C., *Grinding technology: theory and application of machining with abrasives*, Second Ed. Industrial Press: New York, USA, (2008).
[2] Brinksmeier, E., Aurich, J.C., Govekar, E., Heinzel, C., Hoffmeister, H.W., Klocke, F., Peters, J., Rentsch, R., Stephenson, D.J., Uhlmann, E., Weinert, K., and Wittmann, M., Advances in modeling and simulation of grinding processes, *Annals of the CIRP*, 55 (2) (2006) 667-696.
[3] Badger, J.A. and Torrance, A.A., A comparison of two models to predict grinding forces from

wheel surface topography, *International Journal of Machine Tools and Manufacture*, 40 (2000) 1099-1120.

[4] Karkalos, N.E., Markopoulos, A.P., and Dossis, M.F., Application of statistical and soft computing techniques for the prediction of grinding performance, *Journal of Robotics and Mechanical Engineering Research*, 1(2) (2015) 6-16.

[5] Chang, H.C. and Wang, J.J.J., A stochastic grinding force model considering random grit distribution, *International Journal of Machine Tools and Manufacture*, 48 (2008) 1335-1344.

[6] Mishra, V.K. and Salonitis, K., Empirical estimation of grinding specific forces and energy based on a modified Werner grinding model, in: *14th CIRP Conference on Modeling of Machining Operations* (2013).

[7] Agarwal, S. and Rao, P.V., Predictive modeling of force and power based on a new analytical undeformed chip thickness model in ceramic grinding, *International Journal of Machine Tools and Manufacture*, 65 (2013) 68-78.

[8] Karkalos, N.E., Markopoulosa, A.P., and Kundrák, J., Molecular dynamics model of namo-metric peripheral grinding, *Procedia CIRP*, 58 (2017) 281-286.

[9] Zhang, Y., Li, C., Ji, H., Yang, X., Yang, M., Jia, D., Zhang, X., Li, R., and Wang, J., Analysis of grinding mechanics and improved predictive force model based on material-removal and plastic-stacking mechanisms, *International Journal of Machine Tools and Manufacture*, 122 (2017) 81-97.

[10] Durgumahanti, U.S.P., Singh, V., and Rao, P.V., A new model for grinding force prediction and analysis, *International Journal of Machine Tools and Manufacture*, 50 (2010) 231-240.

[11] Lin, K., Xu, X., Li, Y., and Fang, C., Model of grinding force based on stress concentration theory, *Transactions of the Chinese Society for Agricultural Machinery*, 43 (11) (2012) 261-266.

[12] Li, A., Guo, T., Zhang, C., Chen, W., Ye, K., and Lv, Z., *Stress concentration*, China Machine Press: Beijing, China, (1986).